IEEE Access
Multidisciplinary | Rapid Review | Open Access Journal

Received June 3, 2020, accepted June 16, 2020, date of publication June 22, 2020, date of current version July 3, 2020.

Digital Object Identifier 10.1109/ACCESS.2020.3004127

Ultra-Broadband Polarization Conversion Meta-Surface and Its Application in Polarization Converter and RCS Reduction

YUNPING QI[1,2], (Member, IEEE), BAOHE ZHANG[1], CHUQIN LIU[1], AND XIANGYU DENG[1,2]

[1]College of Physics and Electronic Engineering, Northwest Normal University, Lanzhou 730070, China
[2]Engineering Research Center of Gansu Provence for Intelligent Information Technology and Application, Northwest Normal University, Lanzhou 730070, China

Corresponding author: Yunping Qi (yunpqi@126.com)

This work was supported in part by the National Natural Science Foundation of China under Grant 61367005 and Grant 61865008, in part by the Natural Science Foundation of Gansu Province, China, under Grant 17JR5RA078, and in part by the Northwest Normal University Young Teachers' Scientific Research Capability Upgrading Program under Grant NWNU-LKQN-17-6.

ABSTRACT In this paper, an ultra-broadband and high-efficiency polarization conversion metasurface is presented in the terahertz region. The metasureface is similar to a sandwiched structure, which is composed of the top Double Split Ring Resonator (DSRR), an intermediate dielectric layer and a bottom metal layer. Both numerical simulation and theoretical calculation results demonstrate that the proposed metasurface can convert linearly co-polarized waves into cross-polarized waves in the frequency from 2.04 THz to 5.33 THz with a relative bandwidth of 89% and the polarization conversion ratio (PCR) is over 90%. Further simulation results show that the proposed metasurface is insensitive to the polarization angle, and the physical mechanism is revealed in detail by the surface current distribution. In addition, two different kinds of 2-bit coding metasurfaces are designed based on the Pancharatnam-Berry (PB) Phase. The simulated and calculated results show that the proposed PB-coding metasurface has excellent performance in flexibly controlling terahertz wave reflection and low Radar Cross Section (RCS). A 10dB RCS reduction can be achieved from 1.9 THz to 5.5 THz under normal incidence. It provides new degrees of freedom for studying terahertz wave manipulation and reducing RCS.

INDEX TERMS Polarization conversion metasurface, ultra-broadband, Pancharatnam-Berry (PB) phase, coding metasurface, RCS reduction.

I. INTRODUCTION

The polarization state of electromagnetic (EM) wave is one of the characteristics that cannot be ignored in the theoretical analysis and practical applications. Effectively manipulating the polarization state of EM wave is an important direction in scientific research, because it can be applied in numerous electromagnetic applications such as polarizers, beam focusing, vortex beam generation and electromagnetic cloak [1]–[4]. Faraday effect and birefringent crystal are the most principal means for traditional electromagnetic polarization control technology [5], [6]. However, these methods are confronted with limited bandwidth, bulky volumes and not conductive to integrate. In recent years, metasurface which is a two-dimensional metamaterial has attracted increasing attention because its exotic subwavelength micron structure provides unprecedented opportunities to manipulate EM properties [7]–[10]. Since the birth of metasurface, it opens a new technical route for the control of the amplitude, phase, polarization and propagation mode of electromagnetic waves [11]–[13]. Compared with the traditional polarizers, the new polarizers based on the metasurface overcome the shortcomings of the traditional way and exhibit a lot of excellent performances in the manipulation and application of electromagnetic waves [14]–[23], which has attracted extensive attention of academia and industry.

Generally speaking, transmission mode and reflection mode are the most common classification modes of polarization converters. For the transmission mode, chiral metasurface is identified as an effective way and many manipulations of the polarization state have been reported, such as linear to linear [24]–[27], linear to circular [28], [29], and circular to circular [30]. However, narrow operating bandwidth and complex designs extremely limit their practical applications.

The associate editor coordinating the review of this manuscript and approving it for publication was Raghvendra Kumar Kumar Chaudhary.

Reflective polarization converters have important advantages in energy efficiency compared to transmission polarization converters and many structures have been reported, such as V-shaped [31], cut wire shaped [32], [33], L-shaped [34], [1], double U-shaped [35], double W-shaped [36] and double split ring [37]. However, up to now, only a small amount of work can achieve the ultra-broadband, high-efficiency and tractable geometry at the same time, especially in the terahertz region. Radar Cross Section (RCS) is a physical quantity to measure the scattering power of the target to the incident electromagnetic wave in a specific direction. More recently, coding metasurfaces for EM wave manipulation and RCS reduction have been widely studied and many interesting works have been proposed [38]–[41]. Some of them are utilized to reduce the RCS, unfortunately, they have a fixed phase difference once the size of the geometry structure is determined, because the phase gradient in the above method is obtained by gradually changing the size or shape of the geometric. Now a new method is adopted, the reflected terahertz wave can be easily controlled to multiple beams with different degrees of polarization, and the low RCS can be achieved by rotating the different orientation angles of structural unit instead of changing its size.

To address the problem of narrow bandwidth and low efficiency of existing converters, an ultra-broadband and high-efficiency linear polarization converter based on polarization conversion metasurface is designed, which can convert linear polarization to cross polarization in the terahertz region. The results of numerical simulation and theoretical calculation indicate that the converter operates in a wide frequency range of 2.04 THz - 5.33 THZ with polarization conversion rate is above 90%. Moreover, its physical mechanism and insensitivity to the polarization angle were analyzed by simulation. Different from the previous design methods of digital coding metasurface, they manipulating EM wave primarily by designing complex structures or adjusting geometry size parameters. The advantage of PB coding metasurface [42], [43] is to control the terahertz wave flexibly through regular design the rotation angle of the coding elements and coding sequence. Two different kinds of 2-bit coding metasurfaces are proposed and investigated to flexible manipulate terahertz wave reflection and achieve low RCS. It provides a new method for studying terahertz wave manipulation and has huge potential applications from microwave to optics.

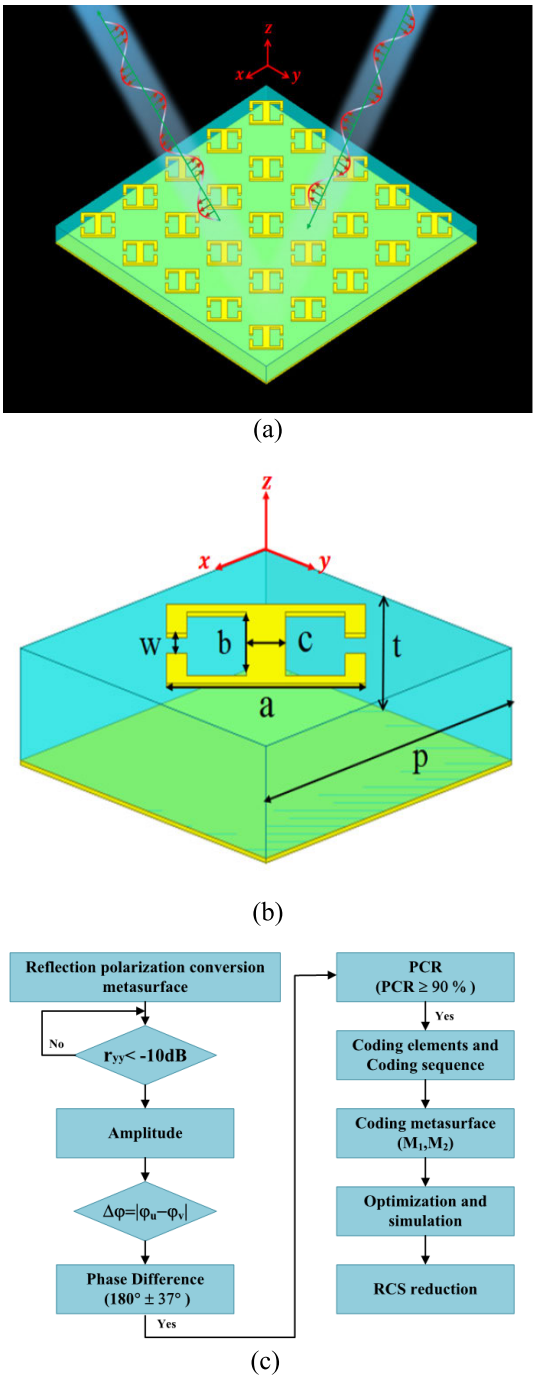

FIGURE 1. (a) The diagram of linear polarization converter, (b) The unit structural parameter of polarization conversion metasurface, (c) The design methodology flowchart of the polarization conversion metasurface and the multi-bit coding metasurface to realize RCS reduction.

II. MODEL DESIGN AND PRINCIPLE

Figure 1(a) illustrates a schematic diagram of the designed linear-polarization converter, which is composed of three parts: the upper layer is made up of the periodic array of the anisotropic Double Split Ring Resonator (DSRR), an intermediate dielectric layer and a bottom metal floor. Copper is selected as the metallic material, with conductivity of $5.8 \times 10^7 S/\mathrm{m}$ and thickness of 240 nm. The polyimide is modeled as a dielectric layer with a thickness of t=11 μm, relative permittivity of $\varepsilon_r = 3$ and loss tangent of $\tan\delta = 0.001$. The size of the top layer structure was optimized by simulation method. The detailed geometric parameters of unit-cell structure by optimized are shown in Fig. 1(b), in which a=20 μm, b=14 μm, c=4 μm, w=6 μm. p=36 μm represents the period of the structure cell. Our target of this work is to realize an ultra-wideband and high-efficiency manipulate terahertz wave and RCS reduction by using the coding PB phase metasurface with the specifically arranged coding sequences. Fig.1(c) gives the design methodology

flowchart of a polarization conversion metasurface and multi-bit PB coding metasurface to realize wide-band RCS reduction. First of all, the key step is to satisfy the conditions of reflection amplitude and phase difference, simultaneously. Because obtain a reflection phase difference of 180° ± 37° is significant to achieve large bandwidth RCS reduction and excellent polarization conversion ratio. Next in importance is the polarization conversion metasurface should have a higher polarization conversion rate. Finally, the simulated results need to be optimized and analyzed to obtain a good performance to accomplish our goal of low RCS in terahertz band.

In order to analyse the polarization conversion performance of our design, the design was simulated by using the finite element method (FEM). Since our structure is symmetrically distributed along an oblique 45° angle, they have the same polarization conversion characteristics when the direction of the incident wave electric field is in the x direction or the y direction. The operating principle of the polarization converter is illustrated in Fig. 2(a). For easy to analyse, we only need to consider the y-polarized EM wave normally incident on the polarization converter during the simulation. The electric field vector can be break down into two perpendicular components along u-axis and v-axis directions, respectively. The incident electromagnetic wave can be expressed as $\vec{E}_i = E_{ui}\widehat{e}_u + E_{vi}\widehat{e}_v$ and the reflected electromagnetic wave can be expressed as $\vec{E}_r = E_{ur}\widehat{e}_u + E_{vr}\widehat{e}_v = r_u E_{ui}\widehat{e}_u + r_v E_{vi}\widehat{e}_v$, in which r_u means the reflected coefficients along the u-axis, and r_v means the reflected coefficients along v-axis. Owing to the anisotropy of the proposed metasurface, this will result in a phase difference $\Delta\varphi$ exists between r_u and r_v of the EM wave reflected by the metasurface. If $r_u = r_v$ and the phase difference $\Delta\varphi \approx 180°$, the direction of the electric field in the u-axis or v-axis direction will be reversed, and the final synthetic fields for E_{ru} and E_{rv} will be along x-axis direction. When the incident plane electromagnetic wave is polarized along the u-axis and v-axis, respectively, the reflection amplitude and phase difference $\Delta\varphi$ are simulated, as depicted in Fig.2 (b). It is clear that the amplitudes of the two reflection curves are nearly equal to 1.0 and the phase difference is approximately 180° ± 37° in the frequency range of 1.9 THz-5.5 THz. The red solid line in the Figure.2 (b) indicates a straight line with a phase of 180°, which has four intersection points with the simulated phase difference curve. The frequencies corresponding to these four intersections are 2.11 THz, 2.78 THz, 3.98 THz and 5.2 THz, respectively. At these four resonance points, the phase difference is equal to 180°, which means significant polarization conversion efficiency can be achieved.

III. SIMULATION RESULTS AND DISSCUSSION

In order to investigate the polarization conversion characteristics of the DSRR in more detail, we define the co-polarization reflection coefficient r_{yy} and the cross-polarization reflection coefficient r_{xy} as $|E_{yr}|/|E_{yi}|$ and $|E_{xr}|/|E_{yi}|$, respectively. Fig. 3(a) gives the simulation analysis results of r_{yy} and r_{xy},

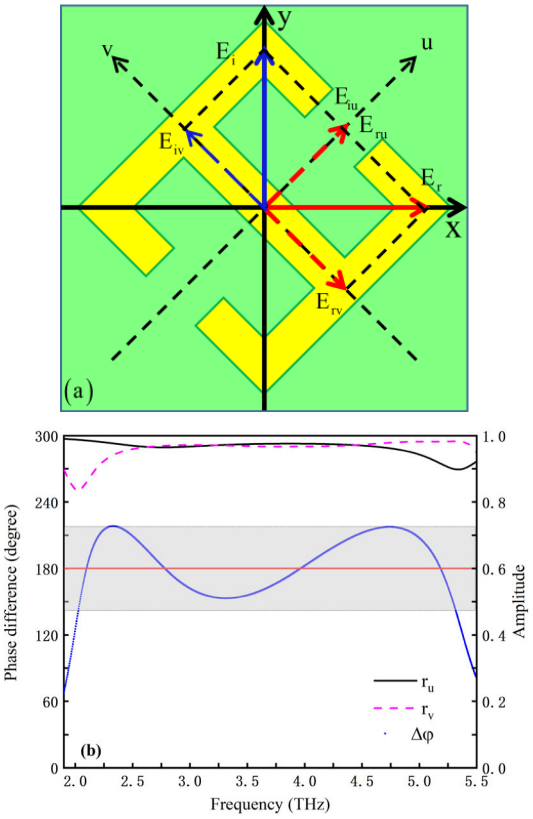

FIGURE 2. (a) The schematic diagram of operating principle, (b) Simulated reflection amplitudes and phase difference of r_u and r_v.

in which the co-polarization reflection coefficient r_{yy} is less than -10 dB and the cross-polarization reflection coefficient r_{xy} is greater than −1 dB in the frequency range from 1.9 THZ to 5.5 THZ, which means that the incident y-polarized wave in this frequency band can be effectively converted into x-polarized wave. PCR is a standard used to assess the performance of polarization converters, because it can more intuitively show the level of polarization conversion, which can be expressed as $PCR_y = r_{xy}^2 \Big/ (r_{xy}^2 + r_{yy}^2)$. Fig. 3(b) gives the calculated PCR. Obviously, in the frequency range from 2.04 THz to 5.33 THz, the PCR is more than 90% and the relative bandwidth is above 89%. Not only that, the PCR reached almost perfect convert efficiency at the above mentioned four resonance frequencies. The above results demonstrate that the proposed polarization conversion metasurface has an excellent polarization conversion performance as well as a wide band.

To better comprehend the physical mechanism of the linear polarization conversion, we then observed the surface current distributions on the top layer structure cell and underlayer metal floor at four resonant frequencies of 2.11 THz, 2.78 THz, 3.98 THz, and 5.2 THz, respectively. In Fig. 4, the direction of the arrows in the figure indicates the direction of the surface current distribution at four resonance frequencies. It can be seen that the surface currents on the top layer of the DSRR is anti-parallel to the underlayer metal floor at

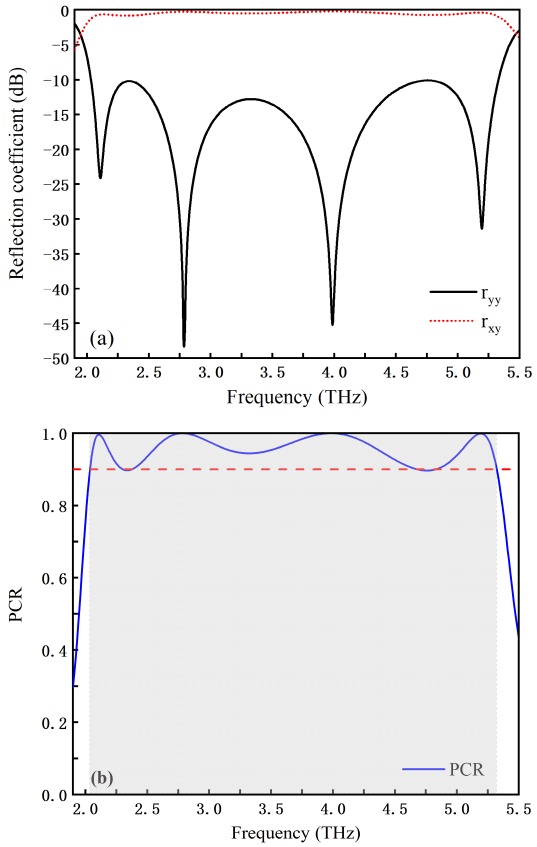

FIGURE 3. (a) Simulated reflection coefficients of r_{yy} and r_{xy}. (b) Simulated PCR of the metasureface.

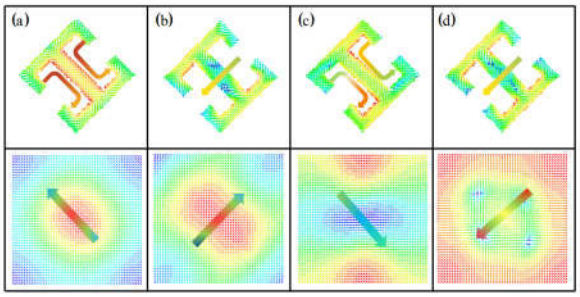

FIGURE 4. Distributions of the surface current on top layer structure cell and underlayer metal floor at the four resonant frequency points. (a) 2.11THz, (b) 2.78THz, (c) 3.98THz, (d) 5.2THz.

2.11 THz and 2.78 THz, respectively. Therefore, the resonances at 2.11 THz and 2.78 THz are caused by magnetic resonances. Different from above, the surface current of the top structure unit is parallel to the underlayer metal floor at 3.98 THz and 5.2 THz, respectively, which is known as electric resonance. The polarization conversion efficiency of broadband originates from the fourth-order electromagnetic resonances of the metasurface. Because of its multiple resonances, these four resonance points play an import role in achieving excellent performance polarization conversion. By adjusting the relative position and quality factor of the

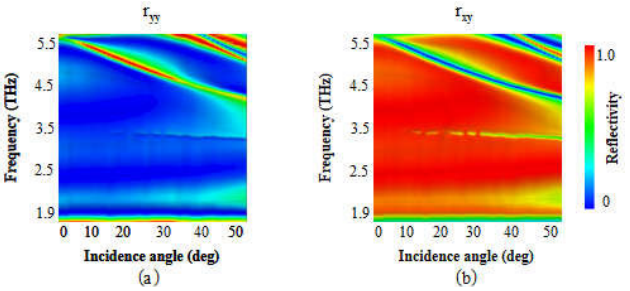

FIGURE 5. The simulated reflection spectra of co-polarization and cross-polarization with the change of the frequency and the incidence angle. (a) r_{yy} (b) r_{xy}.

resonance point, the linear polarization of ultra-broadband can be achieved.

In practical engineering applications, the polarization control of metasurface is often difficult to maintain the electromagnetic wave at normal incidence. Therefore, it is necessary to take the polarization modulation characteristics of metasurface at different incident angles into account. We simulated the reflection coefficients of r_{yy} and r_{xy}, when the angle of incidence changes from 0° to 50° as shown in Figs. 5(a) and (b). It can be observed that r_{yy} can be well kept below 0.1 and r_{xy} maintains a value close to 1.0, which means that our design still has a high polarization conversion efficiency when the incident angle is less than 50°. From Fig.5 we can find that the cross-polarized reflectance decreases slightly at a specific frequency as the incident angle increases in the working frequency band. The destructive interference of metasurface is the main reason for this phenomenon under oblique incidence. As the incident angle increases, the higher the frequency is, the greater the influence of destructive interference is. It is worth noting that the cross-polarization reflectivity decreases sharply with an increase in the incident angle around 3.3 THz and offset to the low frequency band at near 5.3 THz, which means a strong absorption. The reason for this phenomenon may be that the co-polarized reflectance at the corresponding frequency point increases and the absorption of the incident wave increases. This kind of wide-angle and insensitive to the incident angle can provide convenience for practical engineering application.

IV. THEORY ANALYSIS

To further reveal the physical mechanism of the polarization converter, a theoretical analysis is performed. For easy analysis, we only consider the case of normal incidence of y-polarized EM wave. The electric field vector is decomposed into two components in the u-axis and v-axis directions. The incident wave and reflected wave can be described by the following equation (1) and (2), respectively.

$$\vec{E}_i = E_{ui}\hat{e}_u + E_{vi}\hat{e}_v = \frac{\sqrt{2}}{2}\left(\hat{e}_u + \hat{e}_v\right)E_{yi} \tag{1}$$

$$\begin{aligned}\vec{E}_r &= E_{ur}\hat{e}_u + E_{vr}\hat{e}_v = r_u E_{ui}\hat{e}_u + r_v E_{vi}\hat{e}_v \\ &= \frac{\sqrt{2}}{2}\left(r_u\hat{e}_u + r_v\hat{e}_v\right)E_{yi}\end{aligned} \tag{2}$$

TABLE 1. Comparison with other broadband polarization converters in the terahertz region.

Works	Ref.46	Ref47	Ref.48	Ref.49	Ref.50	This paper
OB[a](THz)	0.55-1.37	2.5-3.8	2.9-4.3	0.65-1.58	4.2-5.2	2.04-5.33
RB[b](%)	84	41	39	83	21	89

[a]Operating bandwidth (PCR>90%), [b]Relative bandwidth (PCR>90%)

wherein $\hat{e}_u$ and $\hat{e}_v$ mean the unit vectors in u-axis and v- axis directions, r_u and r_v mean the reflected coefficients along the u-axis and v-axis, respectively. The phases difference between r_u and r_v are represented as $\Delta\varphi$. when $\Delta\varphi = 0°$ or $(\pm 180°)$, the polarization state is liner. when $\Delta\varphi = \pm 90°$, the polarization state is circular polarization. The others represent elliptical polarization. Owing to the anisotropy of the metasurface, there is no polarization conversion in the u-axis and v-axis directions. The relationship between the reflection coefficients in the u-axis and v-axis directions can be expressed as $r_v = r_u e^{j\Delta\varphi}$, and the reflected wave can be rewritten as

$$\vec{E}_r = \frac{\sqrt{2}}{2}\left(\hat{e}_u + \hat{e}_v e^{-j\Delta\varphi}\right) r_u E_{yi} \tag{3}$$

As the reflected wave satisfies the equation

$$\left[E_u^2 + E_v^2 - 2E_u E_v \cos\Delta\varphi = 0.5\left|E_{yi}\right|^2 \sin^2\Delta\varphi\right] \tag{4}$$

According to the electric field relationship of the u-v coordinate system and the x-y coordinate system, Substituting the relationship $E_y = \sqrt{2}/2(E_u + E_v)$ and $E_x = \sqrt{2}/2(E_u - E_v)$, the Eq.4 can be calculated as

$$\frac{E_y^2}{\left|E_{yi}\right|^2 (1+\cos\Delta\varphi)/2} + \frac{E_x^2}{\left|E_{yi}\right|^2 (1-\cos\Delta\varphi)/2} = 1 \tag{5}$$

Equation (5) indicates that the magnitudes of the x-polarized and y-polarized components in the reflected wave are

$$|E_{xr}| = |E_x|_{E_y=0} = |E_{yi}|\sqrt{(1-\cos\Delta\varphi)/2} \tag{6a}$$

$$\left[\left|E_{yr}\right| = \left|E_y\right|_{E_x=0} = \left|E_{yi}\right|\sqrt{(1+\cos\Delta\varphi)/2}\right] \tag{6b}$$

respectively. According to the phase difference $\Delta\varphi$, the eventually cross-polarized reflections r_{xy} and co-polarized reflections r_{yy} can be calculated as

$$r_{xy} = \frac{|E_{xr}|}{|E_{yi}|} = \sqrt{1-\cos\Delta\varphi/2} \tag{7a}$$

$$r_{yy} = \frac{|E_{yr}|}{|E_{yi}|} = \sqrt{1+\cos\Delta\varphi/2} \tag{7b}$$

The phase difference $\Delta\varphi$ of polarization conversion metasurface is simulated by the finite element method as shown in Fig.2 (b). The reflection coefficients r_{xy} and r_{yy} were calculated using the Eq (7a) and (7b). Fig. 6(a) and (b) present the simulated and theoretical calculated results of reflection coefficients and polarization conversion ratio, respectively.

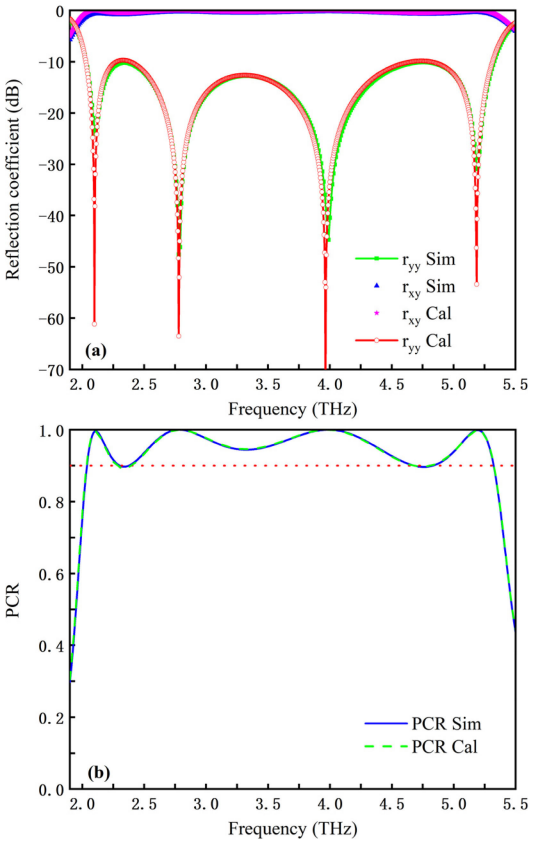

FIGURE 6. Comparison between simulated and calculated results (a) reflection coefficients (b) Polarization conversion ratio.

In Fig. 6(a) the magenta five-pointed starred and the red solid line with a hollow dot indicate the calculated reflection coefficients are r_{xy} and r_{yy}, and the blue triangle and the green solid lines with square marks indicate the simulated reflection coefficients are r_{xy} and r_{yy}. In Fig. 6(b) the solid blue and green dashed lines indicate the simulation and theoretical calculation results of the polarization conversion ratio, respectively. It's clear that the theoretical calculated results are well consistent with the numerical simulations, which further demonstrate that our design has an ultra-broadband and high efficiency in the terahertz region.

Table 1 exhibits the comparison of polarization conversion performance between our study and other recently reported polarization converters in the terahertz regime [43]–[47]. The comparison indicates that our work has an ultra-broadband and high convert efficiently, in which PCR is above 90% in this paper, implying a high performance.

V. DESIGN AND SIMULATION OF CODING METASURFACES

Many researches have confirmed that the PB phase metasurfaces have great potential in electromagnetic wave manipulation and low RCS. The PB phase plays a significant role in the manipulation of circularly polarized (CP) wave. In the case of CP incident, the phase can be controlled by simply controlling the optical axis direction of the structural unit. For brevity, the phase difference $\Delta\varphi$ of CP reflection is closely related to the structure unit rotation angle β, which can be expressed as $\Delta\varphi = \pm 2\beta$, where "+" indicates that the incidence wave is right-handed circularly polarized (RCP) and "−" indicates that the incidence wave is lift-handed circularly polarized (LCP). β is the different rotation angle of the top DSRR as presented in Fig. 7(a). Fig. 7(b) gives the phase relationship of the top DSRR with a different rotation angle β under the incidence wave is LCP. With the increasing of the rotation angle β from 0° to 157.5° with a 22.5° step width, the phase responses gradually increase with a 45° step width and the coverage range is 360° in the operating frequency region. Fig. 7(c) depicts the simulated amplitude for cross-polarization reflection coefficient with different rotation angles under LCP wave normal incidence, respectively. It can be seen that the reflection amplitudes are all remains in a high efficiency for 95% in a wide frequency region 1.9 THz-5.5 THz. The relationship between the eight coding particles and the digital elements of the 1-bit, 2-bit and 3-bit coding PB phase metasurfaces as shown in Fig.7 (d). When the $\Delta\varphi$ of the coding particles is 0° and ±180°, we define such the 0° phase is "0" digital state and the 180° phase is "1" digital state as the 1-bit coding metasurface. For 2-bit coding metasurface, its can produce 0°, 90°, 180°, 270° four reflection phase difference and the corresponding basic digital elements are "00", "01", "10" and "11", respectively. Based on this derivation method, the encoding metasurface can be extended to higher bits, which make the coding sequence more diverse and achieve a wider range of applications.

The principle of manipulating electromagnetic wave by coding metasurface can be explained by the theory of traditional phased array antennas. In the case of plane wave normal incidence, the far-field direction function of the coding metasurface can be described as [49]

$$F(\theta,\varphi) = f_e(\theta,\varphi)\sum_{m=1}^{M}\sum_{n=1}^{N} \times \exp\left\{-i\left\{\begin{array}{l}\varphi(m,n) + kD_x\left(m-\frac{1}{2}\right)\sin\theta\cos\varphi \\ +kD_y\left(n-\frac{1}{2}\right)\sin\varphi\cos\varphi\end{array}\right\}\right\} \quad (8)$$

wherein D_x and D_y represent the length and width of the coding elements along x direction and y direction, respectively. The elevation angle is θ and the azimuth angle is φ, k is the wave-vector in free space, $\varphi(m,n)$ is the reflection phase of coding element. Due to the destructive interference between the coding units, the direction function of grid array $f_e(\theta,\varphi)$

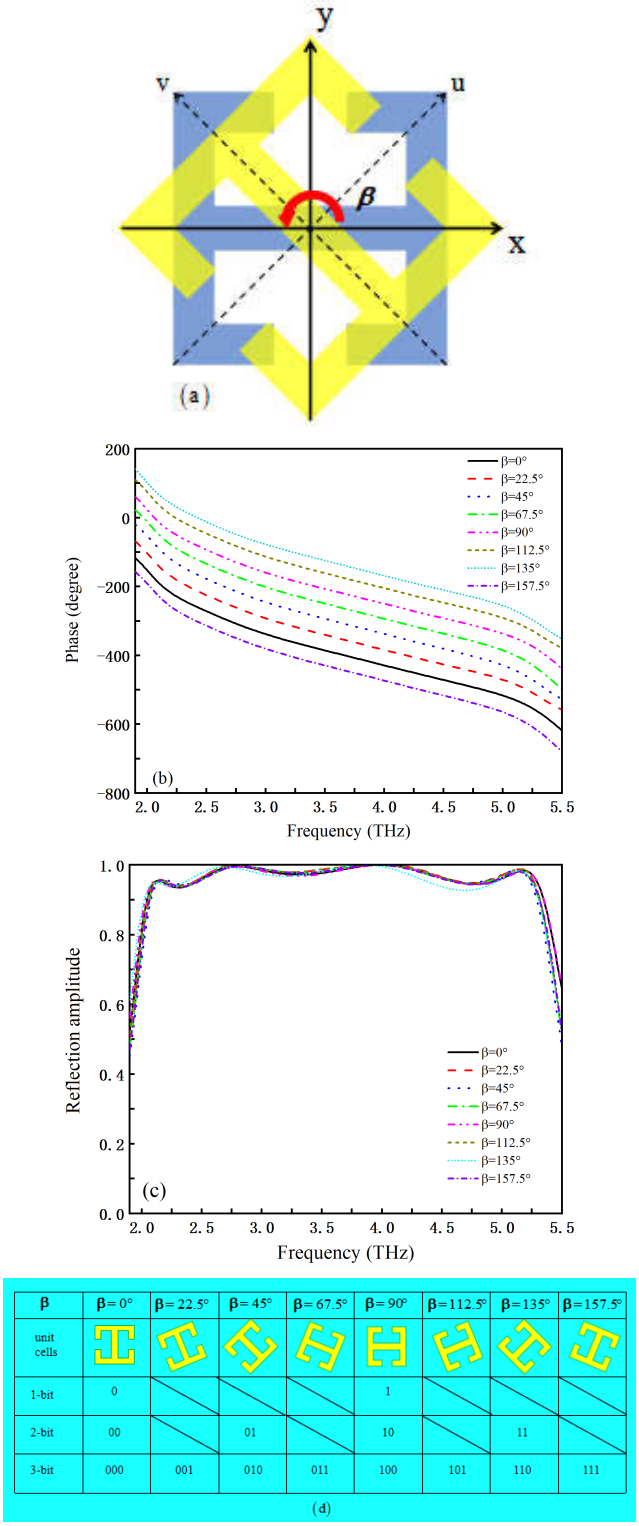

FIGURE 7. (a) The coordinate system and the definition of rotation angle β. (b) Simulated reflection phase of cross-polarization with different rotation angle β under LCP wave incidence. (c) Simulated reflection amplitude of cross-polarization with different rotation angle β under LCP wave incidence. (d) The relationship between the eight coding units and 1-, 2- and 3-bit coding metasurface.

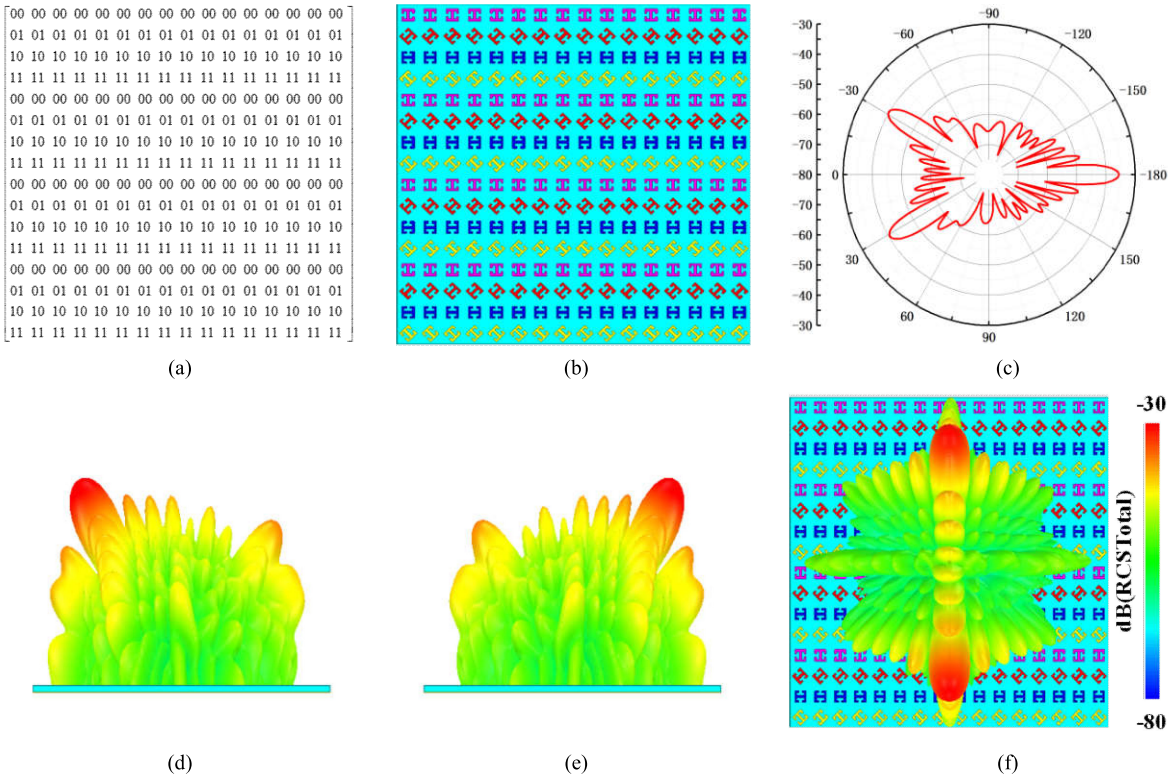

FIGURE 8. (a) 16 × 16 Coding sequences (b) Structures of M_1 metasurface (c)Simulated 2D far-field scattering patterns of the M_1 metasurface under normal incidence of LP wave at 4THz. Simulated 3D scattering patterns of the coding metasurface under normal incidence of (d) RCP. (e) LCP and (f) LP.

is eliminated. Then, the Eq. (8) can be expressed rewritten as

$$F(\theta,\varphi) = \sum_{m=1}^{M} \exp -i\left(kD_x\left(m-\frac{1}{2}\right)\sin\theta\cos\varphi + m\pi\right) \times \sum_{n=1}^{N} \exp -i\left(kD_y\left(n-\frac{1}{2}\right)\sin\varphi\cos\varphi + n\pi\right) \quad (9)$$

where θ and φ can be rewritten as

$$\left\{\begin{array}{l} \varphi = \pm\arctan(\frac{D_x}{D_y})\ and\ \varphi = \pi \pm \arctan(\frac{D_x}{D_y}) \\ \theta = \arcsin\left(\frac{\lambda}{2}\sqrt{\frac{1}{D_x^2}+\frac{1}{D_y^2}}\right) \end{array}\right\} \quad (10)$$

When the designed PB coding metasurfaces are arranged with regularly coding sequence in the same direction, the elevation angle can be simplified as $\theta = \sin^{-1}(\lambda/\Gamma)$. In which λ is the free space wavelength of the incident terahertz wave, and Γ is the physical length of a period of the frequency coding metasurface. The elevation angle θ can be used to check the performance of the designed coding metasurface. By orderly designing the coding sequences of the coding metasurface, the incident energy is redirected to multiple directions and suppresses the energy of each beam, so that the RCS of the metasurface can be effectively reduced.

A. FOR 2-BIT CODING METASURFACE(M_1)

Compared with the 1-bit coding metasurface, the 2-bit coding metasurface has more abundant coding sequences and can be used in a broader range of applications. In order to certify the effectivity of our strategy flexibly manipulate terahertz wave and realize low RCS, two different kinds of 2-bit metasurfaces coding sequences M_1 and M_2 are established. Fig.8 (a) and (b) show the 16 × 16 coding sequences and the structure of M_1 coding metasurface, which is generated with the regularly digital sequence of "00, 01, 10, 11" along y-axis direction. Figure .8 (c) displays the simulated two-dimensional (2D) electric-field scattering patterns under normal incidence of LP wave at the frequency of 4 THz. In the Fig.8 (d)-(f), one can see that the three dimensional (3D) far-field scattering patterns under RCP, LCP, and LP waves normal incidence at the same frequency of 4 THz, respectively. It can be observed that the reflected angles of reflected EM wave at normal RCP and LCP incidences are equal but the direction are opposite. Furthermore, when the LP wave normal incidence the reflected terahertz waves are symmetrically divided into two main lobe beams in the x-z plane, which has the same reflection angle $\theta = \sin^{-1}(\pm\lambda/\Gamma)$. Substituting $\lambda = 75$um(4 THz) and $\Gamma = 144$um, the reflected deviation angle θ can be calculated as 31.38°. Compared with the simulation results in Fig. 8(c), the numerical simulation results agree well with the calculation results. Therefore, by optimizing the coding arrangement sequence of the coding

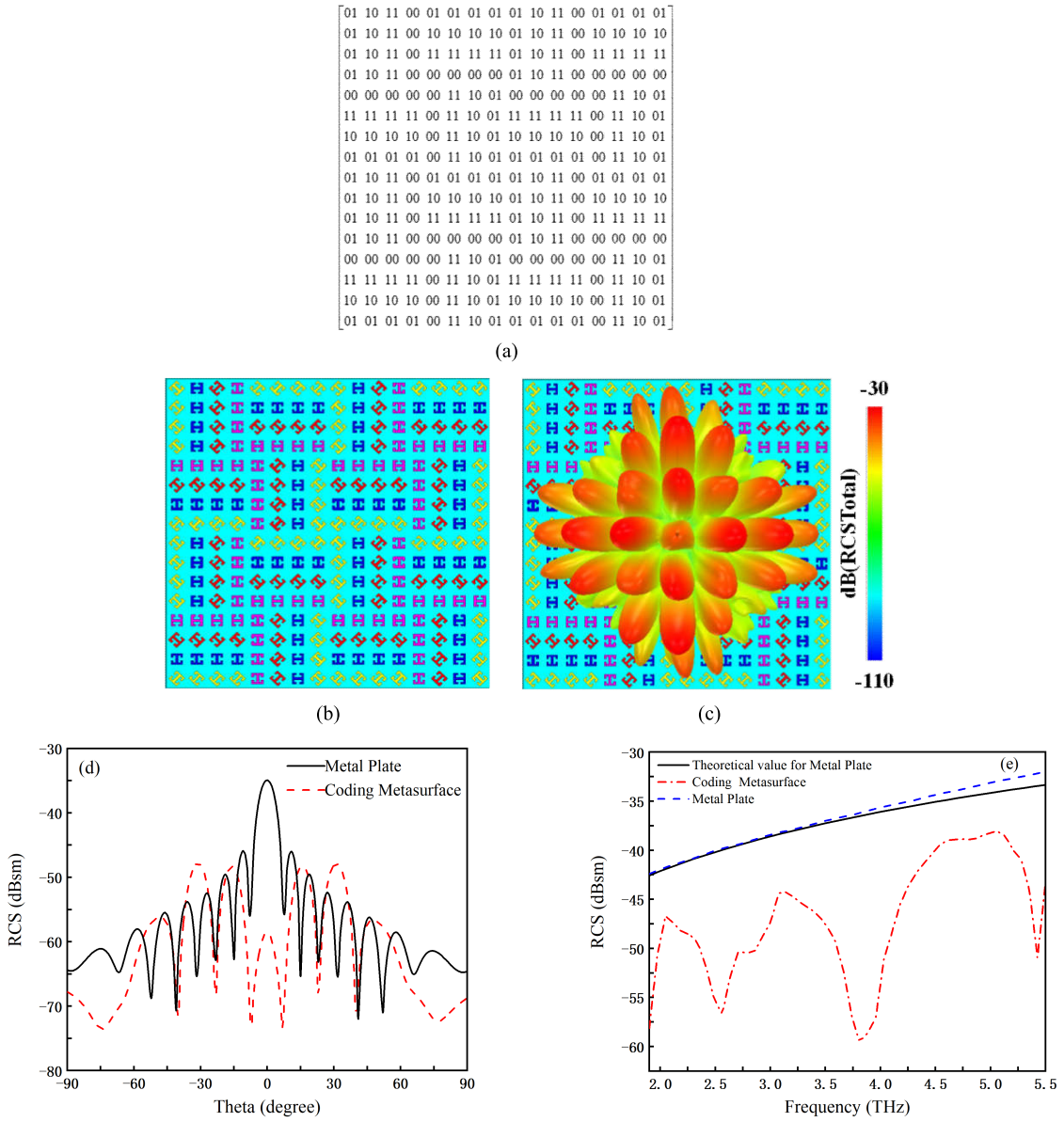

FIGURE 9. (a) 16 × 16 Coding sequences. (b) Structures of M_2 metasurface. The simulated results of coding metasurface M_2 under normal incidence of the LP wave (c) Simulated 3D scattering patterns. (d) Simulated monostatic RCS of coding metasurface M_2 and metal plate at 4THz for phi=0. (e) The values of RCS.

metasurface, the incident terahertz EM wave can be simply and flexibly manipulated. In addition, according to the Eq. (10), when the coding sequence is ready, we can also effectively control the terahertz wave radiation energy with different angles only by changing the working frequency without redesigning the coding sequence of the coding metasurface. All above results confirm that the proposed metasurface has an excellent electromagnetic manipulation capability, which will open a new route to implement multi-beam generation and stealth technology.

B. FOR 2-BIT CODING METASURFACE(M_2)

Based on the above analysis, the incident terahertz wave can be split into multiple directions when the PB coding metasurface is encoded in a specific sequence, which has great potential to achieve low RCS. A new 2-bit coding metasurface(M_2) by optimizing the coding sequence is proposed for low RCS. The coding sequence is illustrated in Fig. 9(a) and the simulated model illustrated in Fig. 9(b). Fig. 9(c) depicts the 3D far-field scattering pattern is simulated under normally incident linearly polarized waves at 4 THz. It clearly presents that the coding metasurface(M_2) diffusely reflects normal incident terahertz waves into numerous different directions in space, and the main lobe energy is dispersed by the side lobe. In order to test whether our design has the ability of reducing RCS, the monostatic RCS of coding metasurface (M_2) and a metal plate with the same size at 4Thz under the normal incidence of LP wave are simulated. The simulation results as shown in Fig. 9 (d). It is worth noting that the RCS reduction is larger than 22.5 dB

within the angle from −15° to 15°. This phenomenon occurs because the PCR of RCS is highly dependent on the incident angles. To further verify the reduction efficiency of RCS, the RCS of metal plate and coding metasurface(M_2) with the same size are simulated under linearly polarized wave normal incidence, as shown in Fig. 9(e). The solid black line means the theoretical RCS of the metallic plate with equal size of the coding metasurface (M_2). The formula for calculation is as follows [50], [51]: $RCS = 10 \times \log_{10}(4\pi l^4/\lambda^2)$, wherein l is the length of the square metallic plate, λ is the free space wavelength of the incident terahertz wave. The blue dotted line and chain dotted red line indicate the simulated result of M_2 under normally incident linearly polarized wave. From Fig. 9 (e), it can be observed that there is a slight error exist between the simulation results and the theoretical values of the metal plate, and the deviation gradually increases as the increase of frequency. Compared with metallic plate, the RCS is reduced more than 10 dB from 1.9 THz to 5.5 THz, which proves our designed 2-bit coding metasurface(M_2) has an excellent capacity of RCS reduction.

VI. CONCLUSION

A terahertz broadband polarization conversion metasurface is proposed and its two application cases are demonstrated by simulation and theory in this paper. Both the numerical simulation and theoretical calculation results indicate that the polarization converter can convert the x- or y-polarized incident wave into cross polarized wave in a wide frequency range of 2.04 THz to 5.33 THz with a relative bandwidth of 89% and the PCR is higher than 90%. Furthermore, its physical mechanism of polarization conversion and insensitivity to the polarization angle are analyzed by simulation. Compared with previous studies, the highlights of the proposed polarization converter are ultra-wideband, high-efficiency and simple geometry. In addition, two different kinds of 2-bit coding metasurfaces are designed based on the PB phase. The simulation results demonstrate that the proposed PB coding metasurface has 22.5 dB RCS reduction, which provides a simple way and more freedom degrees to efficiently control reflected terahertz wave and RCS reduction. We believe that coding metasurfaces will have broad development prospects and huge application potential in microwave, terahertz, and even the visible light.

REFERENCES

[1] T. Guo and C. Argyropoulos, "Broadband polarizers based on graphene metasurfaces," *Opt. Lett.*, vol. 41, no. 23, pp. 5592–5595, Dec. 2016.

[2] H. Shi, J. Li, A. Zhang, Y. Jiang, J. Wang, Z. Xu, and S. Xia, "Gradient metasurface with both polarization-controlled directional surface wave coupling and anomalous reflection," *IEEE Antennas Wireless Propag. Lett.*, vol. 14, pp. 104–107, 2015.

[3] L. Zhang, S. Liu, L. Li, and T. J. Cui, "Spin-controlled multiple pencil beams and vortex beams with different polarizations generated by pancharatnam-berry coding metasurfaces," *ACS Appl. Mater. Interfaces*, vol. 9, no. 41, pp. 36447–36455, Oct. 2017.

[4] M. L. N. Chen, L. J. Jiang, and W. E. I. Sha, "Detection of orbital angular momentum with metasurface at microwave band," *IEEE Antennas Wireless Propag. Lett.*, vol. 17, no. 1, pp. 110–113, Jan. 2018.

[5] S. Ali, J. R. Davies, and J. T. Mendonca, "Inverse Faraday effect with linearly polarized laser pulses," *Phys. Rev. Lett.*, vol. 105, no. 3, Jul. 2010, Art. no. 035001.

[6] X. Zhang, Z. Tian, W. Yue, J. Gu, S. Zhang, J. Han, and W. Zhang, "Broadband terahertz wave deflection based on C-shape complex metamaterials with phase discontinuities," *Adv. Mater.*, vol. 25, no. 33, pp. 4567–4572, Sep. 2013.

[7] W. Sun, Q. He, J. Hao, and L. Zhou, "A transparent metamaterial to manipulate electromagnetic wave polarizations," *Opt. Lett.*, vol. 36, no. 6, pp. 927–929, 2011.

[8] N. K. Grady, J. E. Heyes, D. R. Chowdhury, Y. Zeng, M. T. Reiten, A. K. Azad, A. J. Taylor, D. A. R. Dalvit, and H.-T. Chen, "Terahertz metamaterials for linear polarization conversion and anomalous refraction," *Science*, vol. 340, no. 6138, pp. 1304–1307, Jun. 2013.

[9] H. Chen, J. Wang, H. Ma, S. Qu, Z. Xu, A. Zhang, M. Yan, and Y. Li, "Ultra-wideband polarization conversion metasurfaces based on multiple plasmon resonances," *J. Appl. Phys.*, vol. 115, no. 15, Apr. 2014, Art. no. 154504.

[10] J. Chen, X. Wang, F. Tang, X. Ye, L. Yang, and Y. Zhang, "Substrates for surface-enhanced Raman spectroscopy based on TiN plasmonic antennas and waveguide platforms," *Results Phys.*, vol. 16, Mar. 2020, Art. no. 102867.

[11] H. Shi, A. Zhang, S. Zheng, J. Li, and Y. Jiang, "Dual-band polarization angle independent 90° polarization rotator using twisted electric-field-coupled resonators," *Appl. Phys. Lett.*, vol. 104, no. 3, 2014, Art. no. 034102.

[12] S. L. Jia, X. Wan, P. Su, Y. J. Zhao, and T. J. Cui, "Broadband metasurface for independent control of reflected amplitude and phase," *AIP Adv.*, vol. 6, no. 4, Apr. 2016, Art. no. 045024.

[13] L. Liu, X. Zhang, M. Kenney, X. Su, N. Xu, C. Ouyang, Y. Shi, J. Han, W. Zhang, and S. Zhang, "Broadband metasurfaces with simultaneous control of phase and amplitude," *Adv. Mater.*, vol. 26, no. 29, pp. 5031–5036, Aug. 2014.

[14] Y. N. Jiang, L. Wang, J. Wang, C. N. Akwuruoha, and W. P. Cao, "Ultra-wideband high-efficiency reflective linear-to-circular polarization converter based on metasurface at terahertz frequencies," *Opt. Express*, vol. 25, no. 22, pp. 27616–27623, Oct. 2017.

[15] Y. Qi, Y. Zhang, C. Liu, T. Zhang, B. Zhang, L. Wang, X. Deng, Y. Baia, and X. Wang, "A tunable terahertz metamaterial absorber composed of elliptical ring graphene arrays with refractive index sensing application," *Results Phys.*, vol. 16, Mar. 2020, Art. no. 103012.

[16] Y. Z. Cheng, C. Fang, X. S. Mao, R. Z. Gong, and L. Wu, "Design of an ultrabroadband and high-efficiency reflective linear polarization convertor at optical frequency," *IEEE Photon. J.*, vol. 8, no. 6, pp. 1–9, Dec. 2016.

[17] Y. Jia, Y. Liu, Y. J. Guo, K. Li, and S.-X. Gong, "Broadband polarization rotation reflective surfaces and their applications to RCS reduction," *IEEE Trans. Antennas Propag.*, vol. 64, no. 1, pp. 179–188, Jan. 2016.

[18] H. Wang, Y. Li, H. Chen, Y. Han, S. Sui, Y. Fan, Z. Yang, J. Wang, J. Zhang, S. Qu, and Q. Cheng, "Multi-beam metasurface antenna by combining phase gradients and coding sequences," *IEEE Access*, vol. 7, pp. 62087–62094, 2019.

[19] J.-S. Li and J.-Q. Yao, "Manipulation of terahertz wave using coding Pancharatnam-Berry phase metasurface," *IEEE Photon. J.*, vol. 10, no. 5, pp. 1–12, Oct. 2018.

[20] J. Li, Z. Chen, H. Yang, Z. Yi, X. Chen, W. Yao, T. Duan, P. Wu, G. Li, and Y. Yi, "Tunable broadband solar energy absorber based on monolayer transition metal dichalcogenides materials using au nanocubes," *Nanomaterials*, vol. 10, no. 2, p. 257, Feb. 2020.

[21] Y. Qi, Y. Zhang, C. Liu, T. Zhang, B. Zhang, L. Wang, X. Deng, X. Wang, and Y. Yu, "A tunable terahertz metamaterial absorber composed of hourglass-shaped graphene arrays," *Nanomaterials*, vol. 10, no. 3, p. 533, Mar. 2020.

[22] L. Bao, Q. Ma, G. D. Bai, H. B. Jing, R. Y. Wu, X. Fu, C. Yang, J. Wu, and T. J. Cui, "Design of digital coding metasurfaces with independent controls of phase and amplitude responses," *Appl. Phys. Lett.*, vol. 113, no. 6, Aug. 2018, Art. no. 063502.

[23] X. Yu, X. Gao, W. Qiao, L. Wen, and W. Yang, "Broadband tunable polarization converter realized by graphene-based metamaterial," *IEEE Photon. Technol. Lett.*, vol. 28, no. 21, pp. 2399–2402, Nov. 1, 2016.

[24] Q. Wang, X. Kong, X. Yan, Y. Xu, S. Liu, J. Mo, and X. Liu, "Flexible broadband polarization converter based on metasurfaceat microwave band," 2019, *arXiv:1905.01624*. [Online]. Available: https://arxiv.org/abs/1905.01624

[25] J. Wang, Z. Shen, X. Gao, and W. Wu, "Cavity-based linear polarizer immune to the polarization direction of an incident plane wave," *Opt. Lett.*, vol. 41, no. 2, pp. 424–427, 2016.
[26] H. F. Ma, G. Z. Wang, G. S. Kong, and T. J. Cui, "Broadband circular and linear polarization conversions realized by thin birefringent reflective metasurfaces," *Opt. Mater. Exp.*, vol. 4, no. 8, pp. 1717–1724, Aug. 2014.
[27] S. Sun, W. Jiang, S. Gong, and T. Hong, "Reconfigurable linear-to-linear polarization conversion metasurface based on PIN diodes," *IEEE Antennas Wireless Propag. Lett.*, vol. 17, no. 9, pp. 1722–1726, Sep. 2018.
[28] H. L. Zhu, S. W. Cheung, K. L. Chung, and T. I. Yuk, "Linear-to-circular polarization conversion using metasurface," *IEEE Trans. Antennas Propag.*, vol. 61, no. 9, pp. 4615–4623, Sep. 2013.
[29] H.-F. Zhang, L. Zeng, G.-B. Liu, and T. Huang, "Tunable linear-to-circular polarization converter using the graphene transmissive metasurface," *IEEE Access*, vol. 7, pp. 158634–158642, 2019.
[30] L.-J. Yang, S. Sun, and W. E. I. Sha, "Ultrawideband reflection-type metasurface for generating integer and fractional orbital angular momentum," *IEEE Trans. Antennas Propag.*, vol. 68, no. 3, pp. 2166–2175, Mar. 2020.
[31] X. Gao, X. Han, W.-P. Cao, H. O. Li, H. F. Ma, and T. J. Cui, "Ultrawideband and high-efficiency linear polarization converter based on double V-shaped metasurface," *IEEE Trans. Antennas Propag.*, vol. 63, no. 8, pp. 3522–3530, Aug. 2015.
[32] J. Yang, Y. Cheng, C. Ge, and R. Gong, "Broadband polarization conversion metasurface based on metal cut-wire structure for radar cross section reduction," *Materials*, vol. 11, no. 4, p. 626, Apr. 2018.
[33] Y. Fan, N.-H. Shen, T. Koschny, and C. M. Soukoulis, "Tunable terahertz meta-surface with graphene cut-wires," *ACS Photon.*, vol. 2, no. 1, pp. 151–156, Jan. 2015.
[34] M. Chen, X. Xiao, L. Chang, C. Wang, and D. Zhao, "High-efficiency and multi-frequency polarization converters based on graphene metasurface with twisting double L-shaped unit structure array," *Opt. Commun.*, vol. 394, pp. 50–55, Jul. 2017.
[35] Z. L. Mei, X. M. Ma, C. Lu, and Y. D. Zhao, "High-efficiency and wide-bandwidth linear polarization converter based on double U-shaped metasurface," *AIP Adv.*, vol. 7, no. 12, Dec. 2017, Art. no. 125323.
[36] Y. Zhao, B. Qi, T. Niu, Z. Mei, L. Qiao, and Y. Zhao, "Ultra-wideband and wide-angle polarization rotator based on double W-shaped metasurface," *AIP Adv.*, vol. 9, no. 8, Aug. 2019, Art. no. 085013.
[37] F. Yuan, G.-M. Wang, H.-X. Xu, T. Cai, X.-J. Zou, and Z.-H. Pang, "Broadband RCS reduction based on spiral-coded metasurface," *IEEE Antennas Wireless Propag. Lett.*, vol. 16, pp. 3188–3191, 2017.
[38] L. Jiu-Sheng, Z. Ze-Jiang, and Y. Jian-Quan, "Flexible manipulation of terahertz wave reflection using polarization insensitive coding metasurfaces," *Opt. Expresss*, vol. 25, no. 24, pp. 29983–29992, 2017.
[39] J. Li, X. Chen, Z. Yia, H. Yang, Y. Tang, Y. Yi, W. Yao, J. Wang, and Y. Yie, "Broadband solar energy absorber based on monolayer molybdenum disulfide using tungsten elliptical arrays," *Mater. Today Energy*, vol. 16, Jun. 2020, Art. no. 100390.
[40] J. Han, X. Cao, J. Gao, S. Li, H. Yang, C. Zhang, and T. Li, "Broadband dual-circular polarized coding metasurfaces and their powerful manipulation of differently circular polarizations," *Opt. Express*, vol. 27, no. 23, pp. 34141–34153, 2019.
[41] K. Li, Y. Liu, Y. Jia, and Y. J. Guo, "A circularly polarized high-gain antenna with low RCS over a wideband using chessboard polarization conversion metasurfaces," *IEEE Trans. Antennas Propag.*, vol. 65, no. 8, pp. 4288–4292, Aug. 2017.
[42] B. Lin, J. Guo, L. Lv, Z. Liu, X. Ji, and J. Wu, "An ultra-wideband reflective phase gradient metasurface using pancharatnam-berry phase," *IEEE Access*, vol. 7, pp. 13317–13325, 2019.
[43] Q. Zheng, Y. Li, J. Zhang, H. Ma, J. Wang, Y. Pang, Y. Han, S. Sui, Y. Shen, H. Chen, and S. Qu, "Wideband, wide-angle coding phase gradient metasurfaces based on pancharatnam-berry phase," *Sci. Rep.*, vol. 7, no. 1, Apr. 2017, Art. no. 43543.
[44] X. Jing, X. Gui, P. Zhou, and Z. Hong, "Physical explanation of Fabry–Pérot cavity for broadband bilayer metamaterials polarization converter," *J. Lightw. Technol.*, vol. 36, no. 12, pp. 2322–2327, Jun. 15, 2018.
[45] J. Huang, T. Fu, H. Li, Z. Shou, and X. Gao, "A reconfigurable terahertz polarization converter based on metal-graphene hybrid metasurface," *Chin. Opt. Lett.*, vol. 18, no. 1, 2020, Art. no. 013102.
[46] W. Hong, J. Zhu, L. Deng, L. Wang, and S. Li, "Perfect terahertz-wave polarization rotator using dual Fabry–Pérot-like cavity resonance metamaterial," *Appl. Phys. A, Solids Surf.*, vol. 125, no. 8, p. 519, Aug. 2019.
[47] J. Zhao, Y. Cheng, and Z. Cheng, "Design of a photo-excited switchable broadband reflective linear polarization conversion metasurface for terahertz waves," *IEEE Photon. J.*, vol. 10, no. 1, pp. 1–10, Feb. 2018.
[48] T. Lu, P. Qiu, J. Lian, D. Zhang, and S. Zhuang, "Ultrathin and broadband highly efficient terahertz reflective polarization converter based on four L-shaped metamaterials," *Opt. Mater.*, vol. 95, Sep. 2019, Art. no. 109230.
[49] T. J. Cui, M. Q. Qi, X. Wan, J. Zhao, and Q. Cheng, "Coding metamaterials, digital metamaterials and programmable metamaterials," *Light, Sci. Appl.*, vol. 3, no. 10, pp. e218–e218, Oct. 2014.
[50] Y. Li, J. Zhang, S. Qu, J. Wang, H. Chen, Z. Xu, and A. Zhang, "Wideband radar cross section reduction using two-dimensional phase gradient metasurfaces," *Appl. Phys. Lett.*, vol. 104, no. 22, Jun. 2014, Art. no. 221110.
[51] E. F. Knott, *Radar Cross Section*, 2nd ed. 2004.

YUNPING QI (Member, IEEE) was born in Gansu, China, in 1981. He received the B.S. degree in physics from Northwest Normal University, Lanzhou, China, in 2003, and the M.S. degree in communication and information system and the Ph.D. degree in computational electromagnetics and microwave remote sensing from Beihang University, Beijing, China, in 2006 and 2012, respectively.

From 2008 to 2012, he was a Research Assistant with the Key Laboratory of Electromagnetics and Radio Engineering, Beihang University. Since 2012, he has been an Associate Professor with the College of Physics and Electronic Engineering, Northwest Normal University. His research interests include metasurfaces, RCS reduction, resonances, analytical and numerical methods for guiding, resonant and periodic structures, antennas design, and nanophotonics.

BAOHE ZHANG was born in Gansu, China, in 1993. He received the B.E. degree in communication engineering from Qufu Normal University, Shandong, China, in 2017. He is currently pursuing the master's degree with Northwest Normal University, Lanzhou, China. His research interests include metasurface and antenna designs.

CHUQIN LIU was born in Ningxia, China, in 1994. She received the B.E. degree in biomedical engineering from Nanchang University, China, in 2017. She is currently pursuing the M.S. degree in physical electronics with Northwest Normal University, Lanzhou, China. Her research interests include absorption properties of graphene and metamaterials.

XIANGYU DENG received the B.S. degree in electronic and communications engineering from the Department of Physics, Lanzhou University, Lanzhou, China, in 1998, the M.S. degree in electronic and communications engineering from the Department of Physics, Xidian University, Xi'an, China, in 2005, and the Ph.D. degree in radio physics from Lanzhou University, in 2013. He is currently a Professor with the College of Physics and Electronic Engineering, Northwest Normal University, Lanzhou. His current research interests include digital image processing, artificial neural networks, and pattern recognition.